Thermally Driven Order-Disorder Transition in Two-Dimensional Soft Cellular Systems

Marc Durand[*] and Julien Heu

Matière et Systèmes Complexes (MSC), UMR 7057 CNRS & Université Paris Diderot,
10 rue Alice Domon et Léonie Duquet, 75205 Paris Cedex 13, France

Many systems, including biological tissues and foams, are made of highly packed units having high deformability but low compressibility. At two dimensions, these systems offer natural tesselations of a plane with fixed density, in which transitions from ordered to disordered patterns are often observed, in both directions. Using a modified cellular Potts model algorithm that allows rapid thermalization of extensive systems, we numerically explore the order-disorder transition of monodisperse, two-dimensional cellular systems driven by thermal agitation. We show that the transition follows most of the predictions of Kosterlitz-Thouless-Halperin-Nelson-Young (KTHNY) theory developed for melting of 2D solids, extending the validity of this theory to systems with many-body interactions. In particular, we show the existence of an intermediate hexatic phase, which preserves the orientational order of the regular hexagonal tiling but loses its positional order. In addition to shedding light on the structural changes observed in experimental systems, our study shows that soft cellular systems offer macroscopic systems in which the KTHNY melting scenario can be explored, in the continuation of Bragg's experiments on bubble rafts.

Foams, emulsions, and confluent biological tissues are examples of *soft Cellular systems* (SCS): They are constituted of highly deformable—yet almost incompressible—units (bubbles, drops, cells, etc.), interacting through attractive adhesive interactions and soft steric repulsions. When highly compacted, they tile the available space (3D) or plane (2D) perfectly, i.e., without gaps or overlaps. Interface energy is key to the cohesion and the rigidity of these systems, sometimes constituted solely of fluids. SCS have rough (mechanical) energy landscapes with many local minima: For a given number of units (with prescribed sizes), many different tilings are possible. In some cases the tiling is ordered, consisting predominantly of hexagons (in 2D), and in others it is disordered and includes a distribution of topological defects (polygons with $n \neq 6$ sides). On the timescales considered here, the transition from one local minimum to another is achieved through a succession of elementary structural rearrangements, called $T1$ events [see the inset in Fig. 1(a)], which preserve the integrity and size of the cellular units [1].

Over the past years, special attention has been given to the glass transition in these systems [2–6], i.e., in the transition from a disordered, solid phase to a disordered, liquid phase. In many situations, though—and especially during morphogenetic movements—we observe a transition between ordered and disordered patterns, in both directions [7–12]. Such order-disorder transitions received little attention from a theoretical point of view [13]. In systems that are monodisperse in size, the structural disorder is of topological origin only: For 2D SCS, hexagonal tiling is the only monodisperse regular tiling,

and structural disorder arises from the presence of non-hexagonal cells, or *topological defects*, that are generated by $T1$ events. Structural disorder strongly affects the mechanical properties of a tissue (or any other SCS) and is also essential for its function. Eventually, the study of the pattern of SCS or its fluctuations [14,15] can teach us about its mechanical properties and provide a tool for diagnosis.

In the present Letter, we numerically investigate the order-disorder phase transition in monodisperse 2D cellular systems, using a modified cellular Potts model algorithm that allows thermalization of large systems. Order-disorder transition in SCS is usually driven by a nonthermal source of energy: In a confluent tissue, $T1$'s are consequences of cell activity powered with chemical energy (ATP). In passive SCS such as foams or emulsions, $T1$'s are induced by the injection of mechanical energy through the application of some mechanical stress. Here, we modelize these out-of-equilibrium dynamics by an effective simulation temperature [14] and investigate the phase transition driven by this effective thermal agitation. A thermally driven transition will offer a benchmark system over which we will build up when comparing with actively driven transitions. Since the pioneering Bragg's experiments [16,17], foams and bubble rafts have been recognized as macroscopic model systems for studying the geometry, the dynamics, and the deformation behavior of atomic or molecular materials. We show in the present study that foams also provide a macroscopic model for studying melting of two-dimensional materials.

The order-disorder transition in 2D SCS is reminiscent of defect-mediated theories for melting of two-dimensional
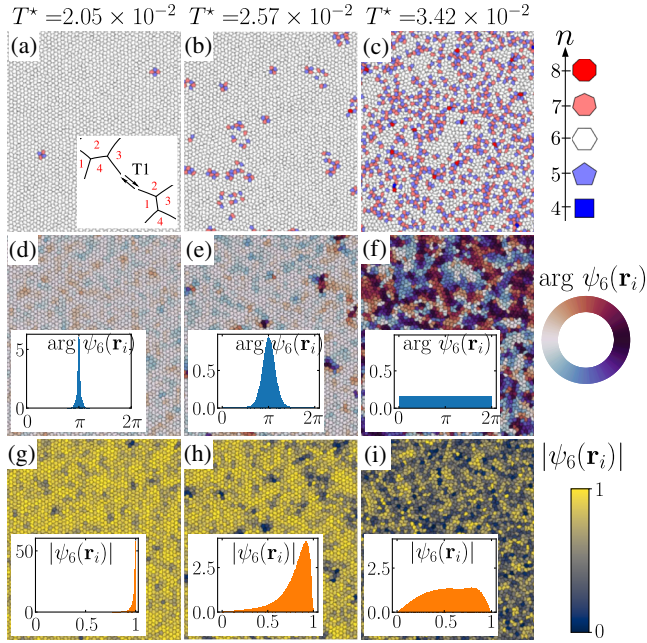
FIG. 1. Evolution of defect populations and orientational order with temperatures. Only a small portion of the system is shown. Columns from left to right: solid, hexatic, and liquid phases. Top row (a)–(c): Population of topological defects. Inset: Sketch of a $T1$ event: In a hexagonal lattice, this topological change corresponds to the creation of a bounded pair of dislocations. Middle row (d)–(f): Phase of the local orientational parameter order $\arg \psi_6(\mathbf{r}_i)$. Insets: Normalized histograms of $\arg \psi_6(\mathbf{r}_i)$, calculated over the whole simulation time. Bottom row (g)–(i): Norm of the local orientational parameter order $|\psi_6(\mathbf{r}_i)|$. Insets: Normalized histograms $|\psi_6(\mathbf{r}_i)|$, calculated over the whole simulation time.

solids. In these theories, the phase transition is described in terms of topological defects in the Voronoi partition associated with the lattice of the solids. Defect-mediated melting theories have been tested, experimentally and numerically, on a large variety of systems, including Lennard-Jones systems [18], colloidal particles [19,20], magnetic beads [21], and disks with either hard-core or soft potentials [22]. SCS yet differ in different aspects from all these classes of systems: First, the partition of 2D space is a physical partition, not a mathematical construction like Voronoi tesselation. Hence, energy and partition are directly related. Second, due to their unique high-deformability–low-compressibility feature, interactions between the cellular units are not pairwise additive [6,23,24]. Many-body interactions are known to affect the mechanical properties of SCS [23]. They also make the phase transition scenario uncertain.

The most popular defect-mediated melting scenario is provided by the Kosterlitz-Thouless-Halperin-Nelson-Young (KTHNY) theory [19,25,26], which predicts two-step melting, from the crystal to an intermediate hexatic phase and then from the hexatic to a liquid phase.

The two transitions are associated with the disappearance of translational and orientational orders, successively. The intermediate hexatic phase has short-range translational order but quasi-long-range orientational order. The dissociation of bound dislocation pairs into free dislocations drives the solid into the hexatic phase, while the unbinding of dislocations into isolated disclinations drives the hexatic to liquid transition. Other melting scenarios are, however, possible. Those based on proliferation of vacancies or interstitials [26] are irrelevant for SCS, in which such defects cannot take place. Another popular scenario argues that, for systems with a core energy of dislocations not too large compared to $k_B T$, melting is caused by the nucleation and proliferation of grain boundaries, preempting the hexatic phase [27,28].

Our simulations are based on the cellular Potts model (CPM), which is widely used for simulating cellular systems in various fields of physics or biology, such as coarsening and mechanics of foams [29,30], tissue morphogenesis [31], cell sorting [32], and collective cell motion in epithelial tissues [33,34]. The CPM is a lattice-based modeling technique: Each cell is represented as a subset of lattice sites sharing the same cell ID (analogical to spins in the Potts model). Cellular domains can adopt any shape on the lattice. The CPM is then particularly suited to simulate thermal fluctuations of cellular systems, as it reproduces realistically the fluctuations of interface locations, even for a wavelength at the subcellular scale. Furthermore, its extension to three dimensions is straightforward. The system evolves using a recently modified Metropolis algorithm that preserves the integrity of the cellular domains and satisfies the detailed balance equation [35], ensuring that the probability distribution of visited states converges to the Boltzmann distribution. This algorithm has also been proved to be more efficient than the standard algorithm used in CPM for the same simulation temperature T [35], allowing us to simulate much larger systems.

Mechanical energy of monodisperse SCS is modeled by the discretized version of the following Hamiltonian:

$$\mathcal{H} = \gamma \sum_{\langle i,j \rangle} L_{ij} + \frac{B}{2A_0} \sum_i (A_i - A_0)^2. \tag{1}$$

The first term in Eq. (1) accounts for interfacial effects: The sum is carried over neighboring cells $\langle i, j \rangle$, and L_{ij} is the boundary length between cells i and j. The second term accounts for an effective area elasticity which results from a combination of three-dimensional cell incompressibility and cell bulk elasticity. B is the effective 2D bulk modulus, A_i is the actual area of cell i, and A_0 is the preferred cell area. This simplified version of the standard Hamiltonian used for cellular systems [5,6,13] corresponds to the situation of a foam or an epithelium with inflated shapes [13,36].

We emphasize that the Hamiltonian (1) cannot be expressed as a sum of pairwise interactions: Because

cellular units have high deformability but low compress-ibility, they adjust their shape rather than their size when brought in contact. In a confluent system, any modification of the interface between cells i and j will imply a displacement of the two cell centers, but also of the other neighboring cells in order to tile the plane perfectly, while preserving cell areas. As a consequence, contact length L_{ij} depends not only on the relative position of the two adjacent cells i and j, but also on the positions of other neighboring cells [6,23,24].

The relative importance of thermal, interfacial, and bulk energies are quantified with two dimensionless parameters: the reduced temperature $T^\star = T/(\gamma a)$ and the reduced compressibility $\xi = \gamma/(Ba)$, where a is the equivalent hexagonal lattice step: $a = (2A_0/\sqrt{3})^{1/2}$. ξ must be low enough to reproduce accurately real systems but must remain finite to allow for some area fluctuations required by the Metropolis-like algorithm.

We have performed extensive numerical simulations of systems of $N = 200^2 = 40\,000$ cells in a rectangular lattice of 1400×1616 sites under periodic conditions (then $A_0 = 56.56$ pixels^2). Periodic boundary conditions allow global translations of the lattice but forbid global rotations. The lattice aspect ratio approximates the target value of $2/\sqrt{3}$, corresponding to the aspect ratio of a perfect hexagonal lattice, with an error of less than $4 \times 10^{-4}\%$. For all simulation runs, we start with the same ordered hexagonal tiling (honeycomb) and wait for equilibration before recording data (see [36] for details on the estimation of equilibration time). In all our simulations, we choose $\gamma = 180$, $B = 200$, and so $\xi \simeq 0.11$.

Figures 1(a)–1(c) show the equilibrated system at three different temperatures, with nonhexagonal cells that are color coded. At a low temperature [Fig. 1(a)], the only topological defects are bound dislocation pairs. At an intermediate temperature [Fig. 1(b)], paired and single dislocations coexist. At a high temperature [Fig. 1(c)], most of the topological defects are assembled into aggregates.

To characterize the static structure of the cellular system occurring during 2D melting, we first calculate the pair correlation function $g(r)$, defined as

$$g(r) = \frac{1}{N}\left\langle \sum_{j \neq k} \delta(r - |\mathbf{r}_j - \mathbf{r}_k|) \right\rangle, \qquad (2)$$

where $\mathbf{r}_j$ and $\mathbf{r}_k$ are the geometric center positions of cells j and k, respectively. The angular brackets denote an average over central cell k. This correlation function gives the probability to find two cells separated by a distance r. Figure 2(a) shows that the peaks of $g(r)$ get broader and shorter as the temperature increases, indicating that the system melts from an ordered crystal to a disordered liquid.

To get more insights into the structural change during the melting process, we focus on the two order parameters
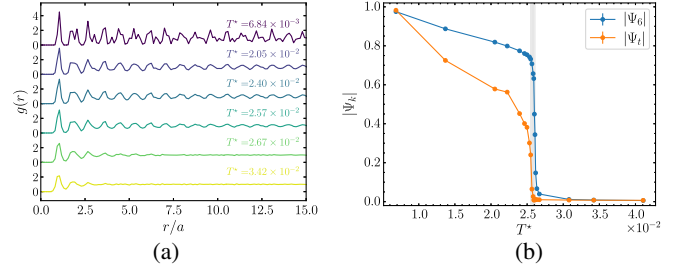

FIG. 2.   (a) Pair correlation function $g(r)$ at different reduced temperatures. Plots are evenly shifted vertically for clarity. Peaks are smeared out as the temperature increases, indicating the loss of translational order. (b) Variation of $|\Psi_t|$ and $|\Psi_6|$ with the temperature. The drop of $|\Psi_t|$ slightly precedes the $|\Psi_6|$ drop, indicating two distinct transitions. The shaded area indicates the existence domain of the hexatic phase as determined from the peaks of the two susceptibilities [see Fig. 4(a)]. Standard errors of the mean are smaller than the size of the markers.

which characterize the translational and orientational sym-metries of the system, respectively. The global translational order parameter is defined by

$$\Psi_t = \frac{1}{N}\sum_{i=1}^{N}\psi_t(\mathbf{r}_i), \qquad (3)$$

where $\psi_t(\mathbf{r}) = \exp(i\mathbf{G} \cdot \mathbf{r})$ is the local translational order parameter for cell i at position $\mathbf{r}_i$ and $\mathbf{G}$ is a primary reciprocal lattice vector. The global orientational order parameter is given by

$$\Psi_6 = \frac{1}{N}\sum_{i=1}^{N}\psi_6(\mathbf{r}_i), \qquad (4)$$

where $\psi_6(\mathbf{r}_i) = (1/z_i)\sum_{j \in z_i} \exp(i6\theta_{ij})$ is the local ori-entational parameter order, z_i is the number of neighbors of cell i, and θ_{ij} is the angle of the bond between centers of cell i and j relative to a fixed reference axis. The magnitude of the local orientational order, $|\psi_6(\mathbf{r}_i)|$ ranges from 0 to 1 and measures the degree to which the cell's neighborhood resembles a hexagonal crystal, while its phase $\arg\psi_6(\mathbf{r}_i)$ indicates the local lattice director.

Spatial distributions of $\arg\psi_6(\mathbf{r}_i)$ and $|\psi_6(\mathbf{r}_i)|$ are shown in Figs. 1(d)–1(i) at three different temperatures. Spatial heterogeneities increase with the temperature. Normalized histograms of $|\psi_6(\mathbf{r}_i)|$ and $\arg\psi_6(\mathbf{r}_i)$ are shown in the corresponding insets. Both quantities are clearly peaked in the solid and intermediate phases, revealing that the orientational order is preserved in these two phases. Peaks are more spread out in the intermediate phase, indicating a quasi-long orientational order in this phase, as expected for the hexatic phase predicted by the KTHNY theory. In the liquid phase, distributions are flat and the orientational order is lost.

Figure 2(b) shows the variation of the global order parameters $|\Psi_t|$ and $|\Psi_6|$ with the temperature. Both curves

present similar tendencies: At a low temperature, both order parameters decay slowly with T. The decay is more pronounced for $|\Psi_t|$, suggesting a quasi-long-range orientational order in the solid phase. Then, both curves drop abruptly to $\simeq 0$. $|\Psi_t|$ falls slightly before $|\Psi_6|$, suggesting the existence of two distinct phase transitions and subsequently the existence of an intermediate hexatic phase, in agreement with the KTHNY scenario.

To further characterize the transition, we now analyze the correlation functions of the two local order parameters, for which specific behaviors are expected within the KTHNY theory [19,25,26]. They are defined as

$$C_k(r) = |\langle \psi_k^*(\mathbf{r'} + \mathbf{r})\psi_k(\mathbf{r'}) \rangle_{r'}| \quad (5)$$

with $k \equiv 6, t$. In Fig. 3(a), $C_t(r)$ shows two different decaying behaviors: For $T^* \lesssim 2.55 \times 10^{-2}$, $C_t(r)$ decays algebraically, which is a signature of a quasi-long-range positional order, and is typical of a 2D solid phase. For $T^* \gtrsim 2.55 \times 10^{-2}$, $C_t(r)$ decays exponentially, revealing a short-range positional order. Near the transition between the two regimes, the power-law exponent is close to $-1/3$, in agreement with the prediction of the KTHNY theory.

In Fig. 3(b), $C_6(r)$ exhibits three different behaviors: At low temperatures ($T^* \lesssim 2.55 \times 10^{-2}$), $C_6(r)$ approaches constants, and the system is in the solid phase with long-range orientational order. At an intermediate temperature ($2.55 \times 10^{-2} \lesssim T^* \lesssim 2.61 \times 10^{-2}$), $C_6(r)$ decays algebraically with an exponent close to $-1/4$, which agrees with the prediction of the KTHNY theory and confirms the existence of a hexatic phase. When the temperature is further increased, $C_6(r)$ decays exponentially and the system becomes a liquid.

To determine more precisely the phase-transition points, we plot the susceptibilities associated with the two order parameters. Unlike correlation functions, the divergence of susceptibility has been shown to be robust to finite-size or finite-time effects. Figure 4(a) shows the variation of the susceptibilities $\chi_k = N(\langle |\Psi_k|^2 \rangle - \langle |\Psi_k| \rangle^2)$ with the temperature.

Their sharp peaks clearly indicate two transitions in the melting process. The peak for χ_t is centered at $T_m^* = 2.549 \times 10^{-2}$, while the peak for χ_6 is centered at $T_i^* = 2.609 \times 10^{-2}$, confirming the existence of an intermediate hexatic phase. It must be emphasized that the values of T_m^* and T_i^* we find are specific to the value of the reduced compressibility ξ chosen for our simulations. The peak for χ_t is much higher than for χ_6, suggesting a continuous solid-hexatic transition and a first-order hexatic-liquid transition. This modified KTHNY scenario has also been observed for systems of hard disks [40].

The KTHNY theory relates the disappearance of translational and rotational orders to dislocations and disclinations unbinding, respectively. To test this scenario, we report in Fig. 5 the evolution of a population of defects with the temperature. The detection and counting of the different defects are detailed in Supplemental Material [36]. As expected, T_m^* coincides with the rapid increase of isolated dislocations due to the dissociation of bound dislocation pairs. On the other hand, the number of disclinations shows a moderate increase around T_i^*. In fact, although the KTHNY scenario assumes that the defects remain diluted during the melting process, in our systems the concentration of defects is such that they form aggregates whose number and mean size increase with the temperature. This aggregation is a natural consequence of the attractive interactions between defects. Aggregates with a nonzero topological charge (i.e., containing unequal numbers of
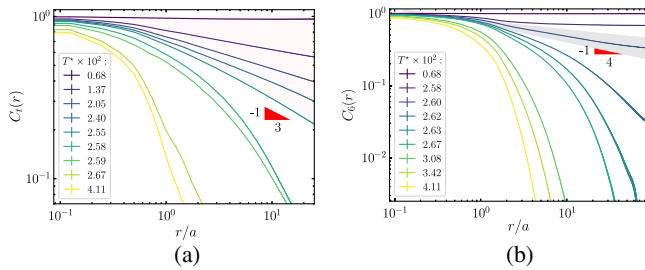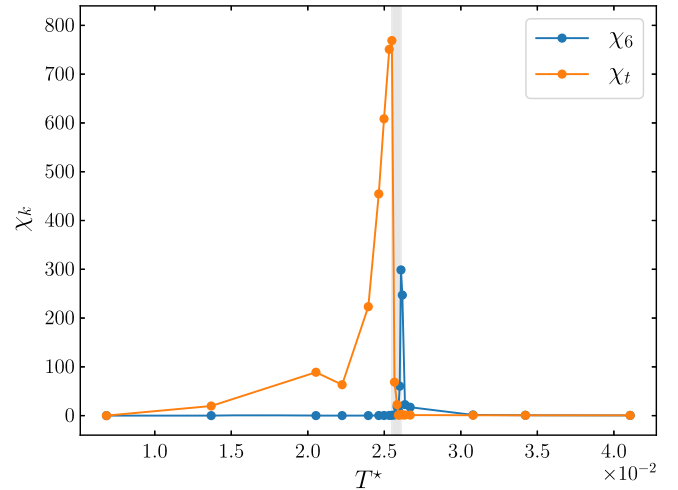

FIG. 3. (a) Translational correlation function $C_t(r)$ in a log-log plot. The curve evolves from a power-law decay (pink area) to an exponential decay as the temperature increases. The $r^{-1/3}$ decaying behavior at the solid-hexatic transition is predicted by the KTHNY theory. (b) Orientational correlation function $C_6(r)$ in a log-log plot. At low temperatures, the curves decay to a plateau. At intermediate temperatures, curves follow a power-law decay (gray area). At higher temperatures, the curves exhibit an exponential decay. The $r^{-1/4}$ decaying behavior at the hexatic-liquid transition is predicted by the KTHNY theory.

FIG. 4. The susceptibilities χ_t and χ_6 as a function of the reduced temperature. The peaks of the translational susceptibility χ_t and the orientational susceptibility χ_6 clearly indicate two transition points, at $T_m^* = 2.549 \times 10^{-2}$ and $T_i^* = 2.609 \times 10^{-2}$, respectively.
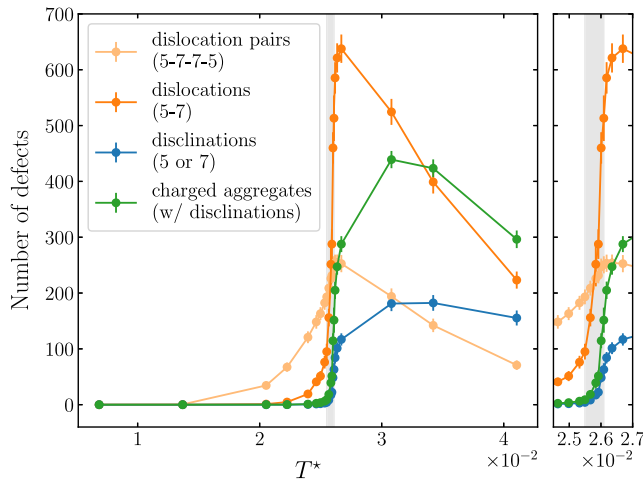
FIG. 5. Number of bound dislocation pairs, dislocations, disclinations, and charged aggregates as a function of the reduced temperature. Right panel: Close-up view showing that the two phase transitions coincide with the rapid increase of dislocations and disclinations + charged aggregates, respectively.

five-sided and seven-sided cells) participate as much as free disclinations in the destruction of the orientational order and, hence, must be accounted for. Figure 5 shows that the population of charged aggregates (including disclinations) increases significantly around $T_i^\star$, in good agreement with the KTHNY scenario.

In summary, we used a recent CPM-modified algorithm that allows for thermalization of large cellular systems and showed that soft cellular systems follow closely the KTHNY melting scenario, hence extending the validity of this theory to systems with many-body interactions. We showed, in particular, the existence of an intermediate hexatic phase. Topological properties of SCS have been mainly characterized by $p(n)$, the proportion of n-sided cells within the system (and many times by the second moment of this distribution solely). Our study shows that $p(n)$ is often not sufficient to capture the mechanical properties of the system, as it can be in a solid, hexatic, or liquid phase. Spatial correlations of defects must also be accounted for. We hope our results will stimulate relevant experimental work to test the existence of an intermediate phase in the order-disorder transitions observed during morphogenetic movements [10–12]. As the defect core energy is the vital predictor of the melting mechanism between KTHNY and grain-boundary scenarios, it would be valuable to quantify the defect core energy of SCS in the future.

[*]marc.durand@univ-paris-diderot.fr

[1] Other structural rearrangements which do not preserve the number and sizes of the cellular units—such as cell division or apoptosis in biological tissues or coarsening in foams and emulsions—usually occur on longer timescales.

[2] T. Aste and D. Sherrington, J. Phys. A **32**, 7049 (1999).

[3] L. Davison and D. Sherrington, J. Phys. A **33**, 8615 (2000).

[4] T. E. Angelini, E. Hannezo, X. Trepat, M. Marquez, J. J. Fredberg, and D. A. Weitz, Proc. Natl. Acad. Sci. U.S.A. **108**, 4714 (2011).

[5] D. Bi, J. H. Lopez, J. M. Schwarz, and M. L. Manning, Nat. Phys. **11**, 1074 (2015).

[6] D. Bi, X. Yang, M. C. Marchetti, and M. L. Manning, Phys. Rev. X **6**, 021011 (2016).

[7] C. Quilliet, S. A. Talebi, D. Rabaud, J. Käfer, S. Cox, and F. Graner, Philos. Mag. Lett. **88**, 651 (2008).

[8] M. Durand, J. Käfer, C. Quilliet, S. Cox, S. A. Talebi, and F. Graner, Phys. Rev. Lett. **107**, 168304 (2011).

[9] M. Durand, A. M. Kraynik, F. van Swol, J. Käfer, C. Quilliet, S. Cox, S. Ataei Talebi, and F. Graner, Phys. Rev. E **89**, 062309 (2014).

[10] J. A. Zallen and R. Zallen, J. Phys. Condens. Matter **16**, S5073 (2004).

[11] A.-K. Classen, K. I. Anderson, E. Marois, and S. Eaton, Dev. Cell **9**, 805 (2005).

[12] A. Hočevar and P. Ziherl, Phys. Rev. E **80**, 011904 (2009).

[13] D. B. Staple, R. Farhadifar, J. C. Röper, B. Aigouy, S. Eaton, and F. Jülicher, Eur. Phys. J. E **33**, 117 (2010).

[14] D. M. Sussman, J. Schwarz, M. C. Marchetti, and M. L. Manning, Phys. Rev. Lett. **120**, 058001 (2018).

[15] E. Fodor, V. Mehandia, J. Comelles, R. Thiagarajan, N. S. Gov, P. Visco, F. van Wijland, and D. Riveline, Biophys. J. **114**, 939 (2018).

[16] W. L. Bragg and J. F. Nye, Proc. R. Soc. A **190**, 474 (1947).

[17] W. L. Bragg and W. M. Lomer, Proc. R. Soc. A **196**, 171 (1949).

[18] K. Chen, T. Kaplan, and M. Mostoller, Phys. Rev. Lett. **74**, 4019 (1995).

[19] H. H. von Grünberg, P. Keim, and G. Maret, in *Colloidal Order: Entropic and Surface Forces*, edited by G. Gompper (Wiley-VCH, Weinheim, 2007), No. 3 in Soft matter, pp. 40–83.

[20] A. H. Marcus and S. A. Rice, Phys. Rev. Lett. **77**, 2577 (1996).

[21] J. Schockmel, E. Mersch, N. Vandewalle, and G. Lumay, Phys. Rev. E **87**, 062201 (2013).

[22] S. C. Kapfer and W. Krauth, Phys. Rev. Lett. **114**, 035702 (2015).

[23] R. Höhler and S. Cohen-Addad, Soft Matter **13**, 1371 (2017).

[24] G. Ginot, R. Höhler, S. Mariot, A. Kraynik, and W. Drenckhan, Soft Matter **15**, 4570 (2019).

[25] K. J. Strandburg, Rev. Mod. Phys. **60**, 161 (1988).

[26] M. A. Glaser and N. A. Clark, *Melting and Liquid Structure in Two Dimensions* (Wiley, New York, 1993), pp. 543–709.

[27] Y. Saito, Phys. Rev. B **26**, 6239 (1982).

[28] S. T. Chui, Phys. Rev. B **28**, 178 (1983).

[29] J. A. Glazier, M. P. Anderson, and G. S. Grest, Philos. Mag. B **62**, 615 (1990).

[30] Y. Jiang, P. J. Swart, A. Saxena, M. Asipauskas, and J. A. Glazier, Phys. Rev. E **59**, 5819 (1999).

[31] T. Hirashima, E. G. Rens, and R. M. H. Merks, Dev. Growth Differ. **59**, 329 (2017).

[32] F. Graner and J. A. Glazier, Phys. Rev. Lett. **69**, 2013 (1992).

[33] A. Szabó, R. Ünnep, E. Méhes, W. O. Twal, W. S. Argraves, Y. Cao, and A. Czirók, Phys. Biol. **7**, 046007 (2010).

[34] A. J. Kabla, J. R. Soc. Interface **9**, 3268 (2012).

[35] M. Durand and E. Guesnet, Comput. Phys. Commun. **208**, 54 (2016).

[36] See Supplemental Material at http://link.aps.org/supplemental/10.1103/PhysRevLett.123.188001 for further details on numerical simulations, which includes Refs. [5,37–39].

[37] N. B. Ouchi, J. A. Glazier, J.-P. Rieu, A. Upadhyaya, and Y. Sawada, Physica A (Amsterdam) **329A**, 451 (2003).

[38] R. Magno, V. A. Grieneisen, and A. F. Marée, BMC Biophys. **8**, 8 (2015).

[39] R. Farhadifar, J.-C. Röper, B. Aigouy, S. Eaton, and F. Jülicher, Curr. Biol. **17**, 2095 (2007).

[40] E. P. Bernard and W. Krauth, Phys. Rev. Lett. **107**, 155704 (2011).